Analysis of bearing steel exposed to rolling contact fatigue

Hansen, K. T.; Fæster, Søren; Natarajan, Anand; Mishin, Oleg; Danielsen, Hilmar Kjartansson; Juul Jensen, Dorte; Klit, Peder

Published in:
I O P Conference Series: Materials Science and Engineering

Link to article, DOI:
10.1088/1757-899X/219/1/012024

Publication date:
2017

Document Version
Publisher's PDF, also known as Version of record

Analysis of bearing steel exposed to rolling contact fatigue

K T Hansen[1], S Fæster[2*], A Natarajan[2], O V Mishin[2], H K Danielsen[2], D Juul Jensen[2] and P Klit[1]

[1] Department of Mechanical Engineering, Technical University of Denmark 2800 Kgs. Lyngby, Denmark
[2] Department of Wind Energy, Technical University of Denmark, Risø Campus, 4000 Roskilde, Denmark

*E-mail: sfni@dtu.dk

Abstract. The objective of this work is to characterize fatigue damage in roller bearings under conditions of high load and slippage. A test rig constructed for rolling contact fatigue tests of rings is described, and test results are presented for rings taken from two spherical roller bearings. The preparation of the rings and the loading situation are explained. Test conditions are chosen with the aim of achieving pitting formation at the contacting surfaces. During testing the contact pressure, torque and the rotational speed are monitored and recorded. After testing the tested rings have been characterized using X-ray tomography and scanning electron microscopy. The observations confirm that rolling contact fatigue testing at high loads leads to pitting failure at the contacting surfaces. The pitting mostly appears on one side of the contact, attributed to a non-uniform contact pressure in the axial direction.

1. Introduction

Bearings in wind turbine drivetrains operate under highly dynamic conditions, even during normal operation. This is due to the interaction of the wind turbine rotor with wind turbulence, wind shear and yaw, which result in varying cyclic loads on the main shaft. The drivetrain configuration can be based on either a 3-stage high speed geared transmission, a medium speed transmission or a direct drive (gearless). In all cases, the main shaft is connected to the rotor hub through one or two main bearings. The conventional drivetrain configuration has the generator and converter behind the tower [1]. In some large direct drive gearless configurations, the main bearing, along with the generator, is bolted to the hub, thus front-mounting the entire drivetrain to reduce deflections [1]. Nevertheless, the main bearings and/or gearbox bearings are always loaded dynamically in the axial and radial directions.

Several tests have been carried out both in test facilities [2] as well through direct measurements on wind turbines [3] regarding drivetrain loading conditions for the validation of load simulations and the design process. The Gearbox Reliability Collaborative [2] instigated by the National Renewable Energy Laboratory in the USA, has been a multi-year effort, where loads at the bearings of a 3-stage planetary gearbox of a 750 kW wind turbine drivetrain were measured in a test facility under different transient conditions. While the tests validated multi-body model predictions of drivetrain loads, they also revealed the role played by bearing lubrication and slippage of rollers inside the bearings on accelerating bearing damage and roller fatigue.

Wind turbine gearbox and bearings are designed as per the IEC 61400-4 standard [4], following the load conditions prescribed in IEC 61400-1 [5]. Several design load cases, such as normal stops, emergency stops, grid outage, and start-ups, as realistically experienced by a turbine, result in highly

transient loads in the gearbox bearings. The roller bearings in such cases may be momentarily underloaded, i.e., a situation where there is insufficient contact force between the rollers and the inner raceway, resulting in sliding of the rollers and subsequent impact upon re-contact [6]. Other extreme load situations, depending on the action of the turbine control system during extreme events, can result in extreme contact stresses inside bearings [7], which may exceed the permissible contact stress limits of the bearing.

This contact between the roller and the raceway is usually modelled as a line contact for roller bearings [7]. Accordingly the maximum contact stress depends on the radial load, the diameter of the raceway, the diameter of the roller and its width. The contact stiffness of the bearing increases with increasing bearing size, if the turbine is upscaled. Therefore, for a fixed turbine size and rating, increasing the diameter of the bearing can reduce the contact stress experienced by the bearing during extreme events. As per the IEC 61400-4 standard, the contact stresses should be below 2.5 GPa for bearings up to a 500 mm inner raceway diameter. While this is the ultimate contact stress limit, the rolling contact fatigue (RCF) load limit depends on the number of load cycles, the rotational speed variations of the bearing and the wear of the surface. The roller or raceway surface wear is difficult to quantify numerically, since it depends on lubrication quality, surface roughness, pre-existing defects etc., but the presence of wear may significantly reduce the rolling fatigue lifetime.

The aim of the present work is to set up a laboratory facility for the testing of RCF of gearbox bearings under controlled load, sliding and lubrication conditions. In this paper the test set-up is described, and preliminary results are presented. The surface of a bearing ring subjected to RCF in the new test facility also is characterized using X-ray tomography and scanning electron microscopy.

2. Experimental

2.1. *Description of the rolling contact fatigue testing machine*

A test rig for RCF of bearing steel under conditions similar to those in modern wind turbines has been constructed at the Department of Mechanical Engineering at the Technical University of Denmark. In the test rig, two drive shafts are forced together by a hydraulic cylinder (figure 1). By positioning a ring on each of the two individual shafts the outer surfaces of the rings can be brought together. The surface of both rings therefore corresponds to the inner ring in a bearing. The revolutions per minute of the two shafts are controlled individually to create rolling, as well as sliding, conditions. A lubrication inlet is positioned just above the position at which the two rings contact each other, and the amount of lubricant flowing into the contact is controlled. The interfacial torque generated between the two surfaces is measured by a torque transducer attached to drive shaft 2 (see figure 1).

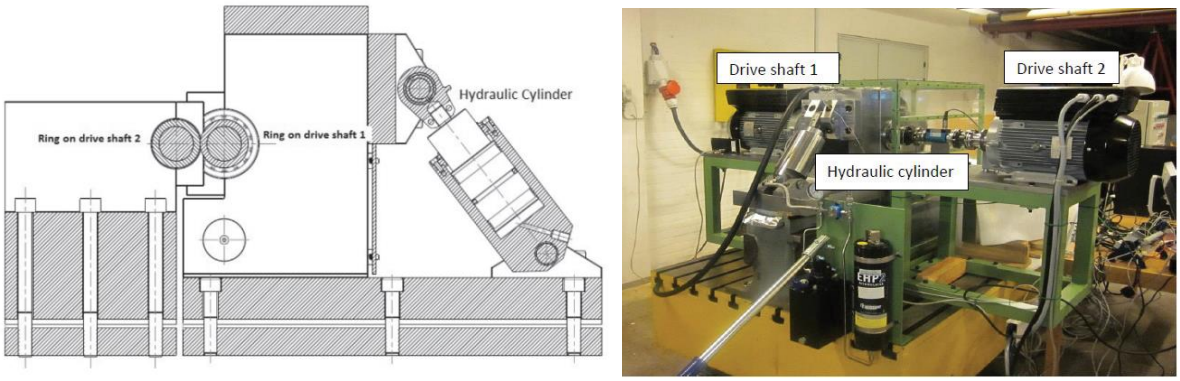

(a) (b)

Figure 1. The test rig used in the present experiment: (a) schematic illustration; (b) photographic image.

2.2. *Material and rolling contact fatigue testing conditions*

The rings used in the present experiment were taken from two spherical roller bearings received from SKF (figure 2). Both rings were removed by breaking the roller cage and removing enough rollers to loosen the inner ring. The desired contact area shown in figure 2(a) was ground on both rings. One ring was ground to a width of 5 mm, while the other was ground to a width of 3 mm. This was done to prevent two opposing edges rolling against each other. These rings are in the following termed the 5-mm ring and the 3-mm ring, respectively. The contact diameters of the rings were 75.84 mm for the 3-mm ring and 75.33 mm for the 5-mm ring. The cross-section of the intended line contact is shown in figure 2(b). This contact is comparable to the contact in the roller bearing.

Both rings were pressed onto their respective shafts until a diametrical expansion of 0.12 mm was achieved on each ring, as measured by the contact diameter. This expansion approximately corresponds to a fitting pressure of 132 MPa for the 5-mm ring and 135 MPa for the 3-mm ring at 2000 rpm and 20 °C [8]. The difference in fitting pressure is due to the difference in the unexpanded contact diameter, as the ring with the larger diameter (3-mm ring) requires a higher fitting pressure in order to expand the outer diameter by 0.12 mm. Both shafts were installed in the test rig, and their axial positions were adjusted using shim washers and wave springs to achieve about 1 mm of clearance on each side of the 3-mm ring. After the shafts were installed, the roundness, measured using a 0.01 mm dial indicator, was 0.02 mm for the 5-mm ring and 0.01 mm for the 3-mm ring.

The lubricant used in the present experiment was the fully synthetic Mobil Delvac gear oil 75W-140, which is a heavy duty drivetrain lubricant with a viscosity of 182 cSt at 40 °C and 25 cSt at 100 °C. Droplets of the lubrication fell freely into the contact zone between the two rings. The target contact pressure for the tests performed was chosen to be 3.5 GPa to ensure relatively fast pit formation.

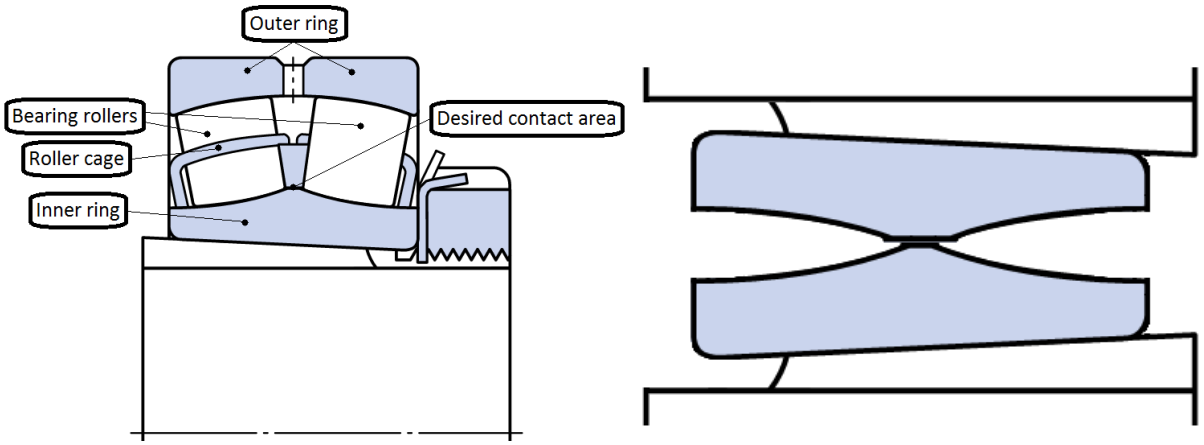

Figure 2. Schematic illustration of bearings applied in the present experiment: (a) cross-section of the bearing; (b) cross-section of the inner rings ground to the desired contact width.

2.3 Roughness and hardness measurements, tomography and microscopy

One 5-mm ring containing a coarse pit after RCF testing was characterized in the present work. The surface roughness Ra was first measured over a length of 5 mm on the contact surface, avoiding pitted areas. Vickers hardness measurements were then made both on the contact surface and along the mid-thickness in the cross-section of the ring. The load applied was 1 kg, with a dwell time of 15 s.

Two samples were then machined from the ring in the location of the pit and from the opposite side of the ring, and 3D X-ray tomography scanning was performed on both samples using a Zeiss Xradia 520 Versa. The scans were performed using a polychromatic beam with energies up to 160 kV from a tungsten target. 3D density maps were reconstructed by a standard filtered back projection based on a Feldkamp algorithm [9] from 3201 projections obtained during a 360° rotation of the sample. The

reconstructions covered a 2k × 2k × 2k voxel volume, with a voxel size of 7.67 µm. 3D volumes were segmented and visualized using the Avizo software package. The outer surface of the samples was also inspected using a Zeiss Supra 35 scanning electron microscope (SEM).

3. Results and Discussion

3.1. Rolling contact fatigue test data

The force applied from the hydraulic loading arrangement during the RCF test is shown in figure 3. In this figure, the target force is represented by a black line, and a ±4.62 MPa range below and above the target is marked, which corresponds to ±50 N. The moving average (MA), calculated over a duration of 300 seconds, is mostly within the target range over the entire dataset. However as it is necessary to adjust the force manually during testing, the force occasionally drifts out of this range. The abrupt vertical increases and drops seen in figure 3 correspond to starting up and shutting down of the test rig. Based on the MA, it is concluded that the rings were mostly subjected to ~3.5 GPa contact pressure.

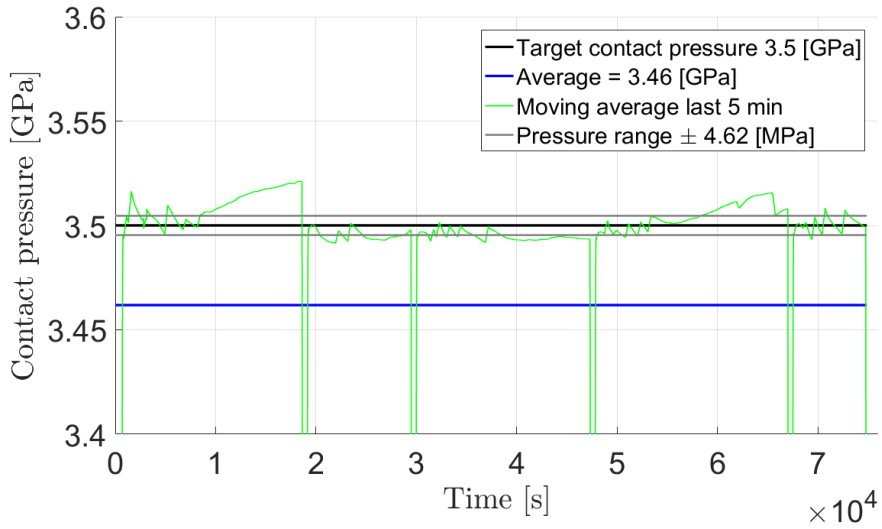

Figure 3. The applied contact pressure as a function of time.

Figure 4 shows the complete torque history for the entire RCF test. Although the torque should ideally be zero for pure rolling, there are small variations in the operating speed of each drive. These variations originate from the frequency converters controlling the drives, as they do not supply a steady frequency. Again, the steep changes seen periodically in the MA of the torque are due to start-up and shut-down of the test rig. It is clear from figure 4 that the test rings experienced some slip during the test. However, considering that the maximum deviation seen in figure 4 is only 0.6 Nm, the level of slip is small.

The rotational speed of each drive is shown in figure 5. It is evident there was a difference in the speed of the two drives, arising from the different contact diameters of the test rings. The rotational speed of each drive is, however, considered to be close enough to the goal of 2000 rpm. The periodic sudden increases in speed originate from start-up of the test rig, and are seen to decrease within a short period of time as the steady state operating speed is achieved. The graphs in figure 5 demonstrate similar patterns, which in combination with the applied torque data (figure 4), indicates that during the test the conditions of the rings were fairly close to pure rolling.

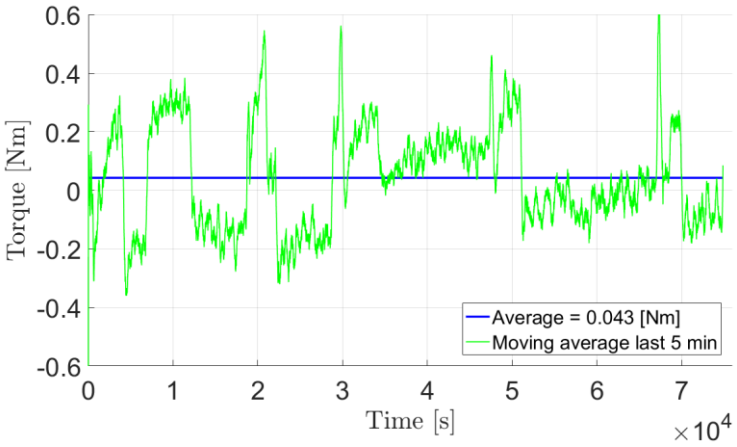

Figure 4. The torque transmitted as a function of time.

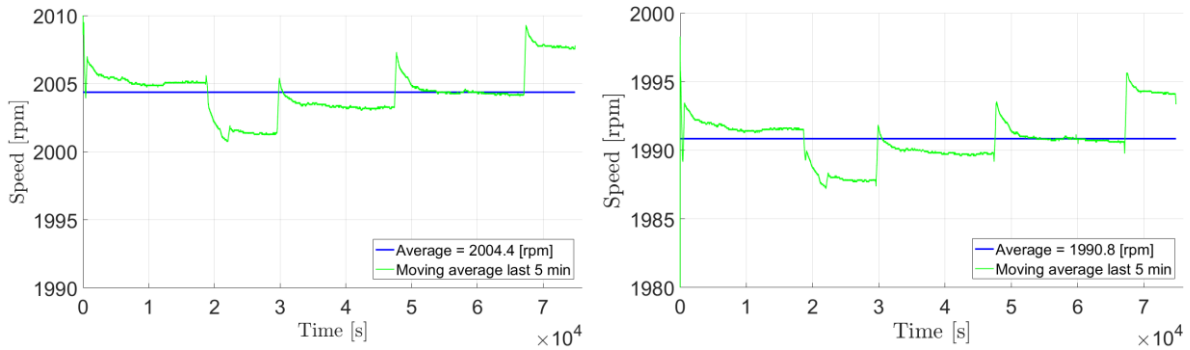

(a) (b)

Figure 5. Rotational speed as a function of time: (a) drive 1; (b) drive 2.

Table 1 shows the total contact time of the ring pair during test operation before pitting failure occurred, as well as the total number of revolutions of the individual rings, the mean of each adjustable parameter, and the surface roughness Ra measured after the test at locations away from the pitted area. The Ra values indicate that the surfaces (except for the pitted areas) are similar to those after the initial grinding, for example, Ra values measured on the 5-mm ring before and after the test are 0.6 µm and 0.69 µm, respectively. As can be seen in table 1, the total number of revolutions exceeded 10^6, which indicates that the test pieces entered the high cycle fatigue range. Thus, the load conditions for the laboratory experiment are comparable to actual loading conditions for bearings in operation.

Table 1. Data for the entire test run to maintain the maximum contact pressure of 3.5 GPa.

Parameter	Number	Unit
Total time	20:47:53	hh:mm:ss
Total no. of revolutions (drive 1)	2,526,662	r.
Total no. of revolutions (drive 2)	2,509,550	r.
Mean force	18,667	N
Mean torque	0.04	Nm
Mean speed (drive 1)	2,004	rpm
Mean speed (drive 2)	1,991	rpm
Ra (5-mm ring)	0.69	µm
Ra (3-mm ring)	0.52	µm

3.2. Hardness data and defect observations

The average Vickers hardness measured on the contact surface is 800 HV1, which is greater than that measured along the ring mid-thickness of 740 HV1. Thus, the contact surface was hardened considerably during the test.

X-ray tomography images from the outer surface of the 5-mm ring are shown in figure 6. A circumferential groove with a depth of 35 µm is observed (marked by arrows) near one edge of the contact surface both in the pit-free sample (figure 6(a)) and in the sample with the coarse pit (figure 6(b)). Apparently, this groove extends over the entire ring circumference. The groove originates from the contact between the edge of the 3-mm ring and the 5-mm ring, and results from an angular misalignment between the two ring surfaces caused during the grinding process, which leads to conical contact between the two rings mainly along this groove. This was confirmed by inspecting another pair of rings, where it was found that the centre axis of the grinding stone was not properly aligned with the centre axis of the test piece. This resulted in a conical shape of the contacting surface with an inclination angle of 0.88°. Some degree of variation between the slopes is common since each ring is ground separately, but this variation is small compared to the magnitude of the misalignment. The conical shape greatly changes the contact situation, which ideally should have been a 3-mm wide line contact. The contact pressure was thus much higher at one end of the line contact than originally planned. As a result of the high contact pressure, it is likely that plastic yielding occurred in both rings, widening the contact area during the test.

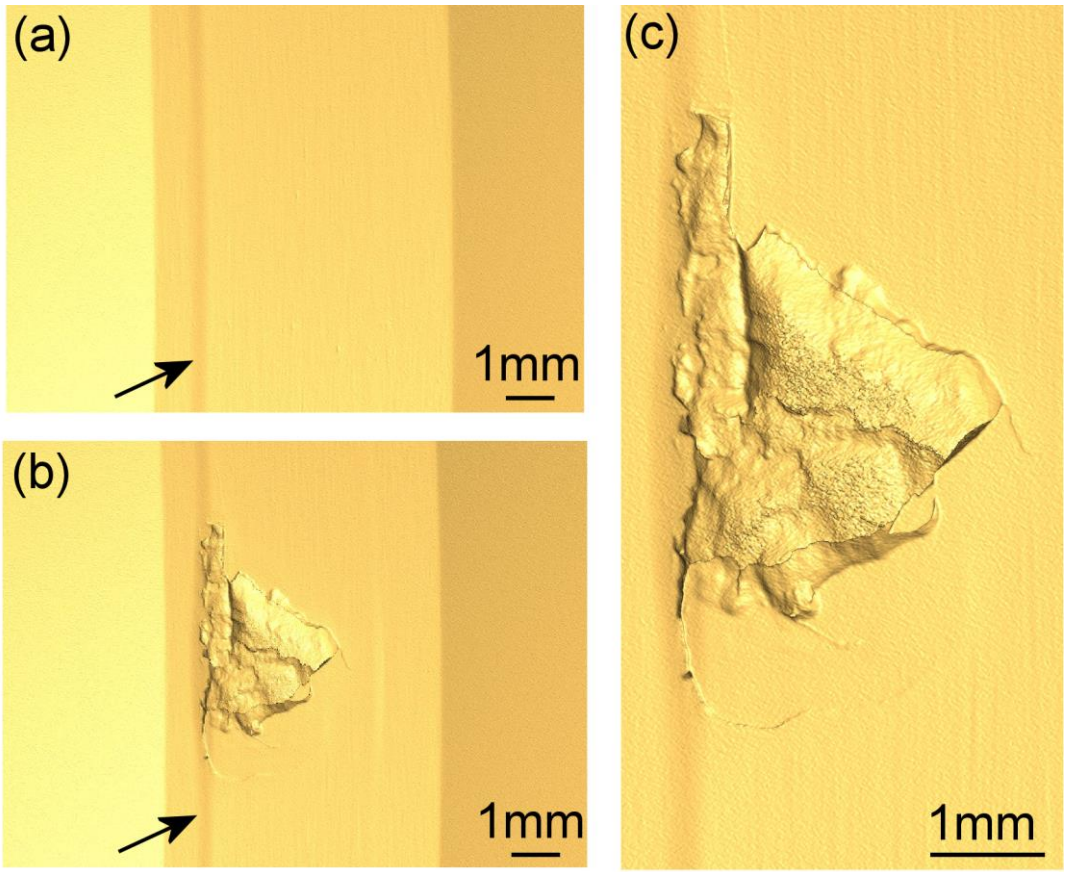

Figure 6. X-ray tomography images from two samples machined from opposite sides of the tested 5-mm ring: (a) pit-free sample; (b,c) sample with a coarse pit, which is shown at low (b) and higher (c) magnifications. The groove corresponding to the high pressure region extending over the entire ring circumference is marked by arrows in (a,b).

The size of the pit shown in figure 6(b) is ~3 mm, and the depth is 420 µm. Since the pit is widest in the vicinity of the circumferential groove, it is suggested that the pit starts propagating from this groove. A SEM image in figure 7(a) shows the central portion of the coarse pit, where multiple cracks are seen both near the pit and on the pit surface. Cracks are also observed at some distance from the pit, but still close to the edge of the contact surface (see figure 7(b)). The defects observed on the contact surface appear to be examples of damage associated with classical pitting failure.

The RCF test was stopped when the vibration level increased significantly, due to the development of the coarse pit shown in figure 6(b,c) and figure 7(a). The cracks along the contact zone show, however, that more pits had started to develop before the RCF test was stopped. It is suggested that the cracks started below the surface, where the shear stress had its maximum value. Furthermore, SEM inspection reveals cracks on the contact surface even in the pit-free sample. Figure 8 shows an X-shape crack with arms extending over at least 0.5 mm, observed near the circumferential groove marked in figure 6(a). This crack is apparently very shallow and thus not observable in the X-ray tomography image in figure 6(a). Such cracks are considered to be precursors of pits.

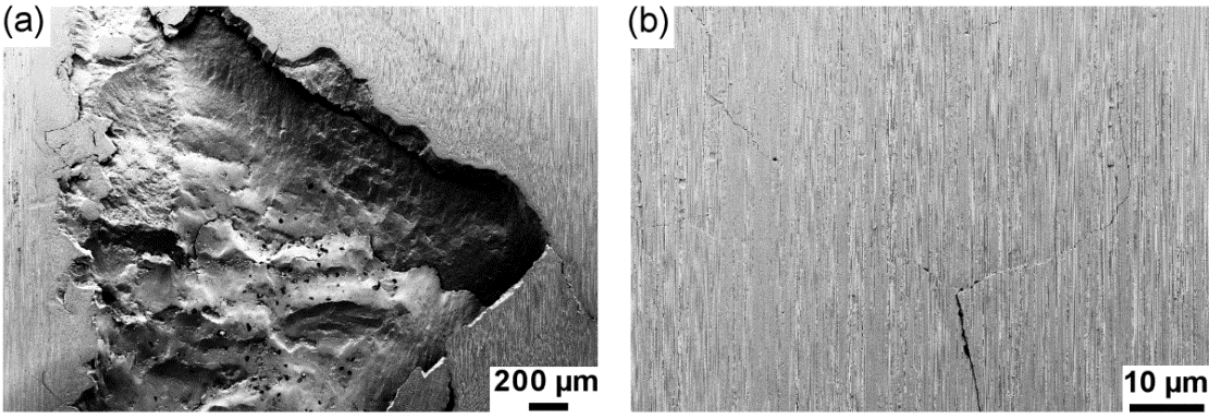

Figure 7. SEM images from the sample containing the coarse pit: (a) central part of the pit; (b) cracks far away from the pit, but still near the groove.

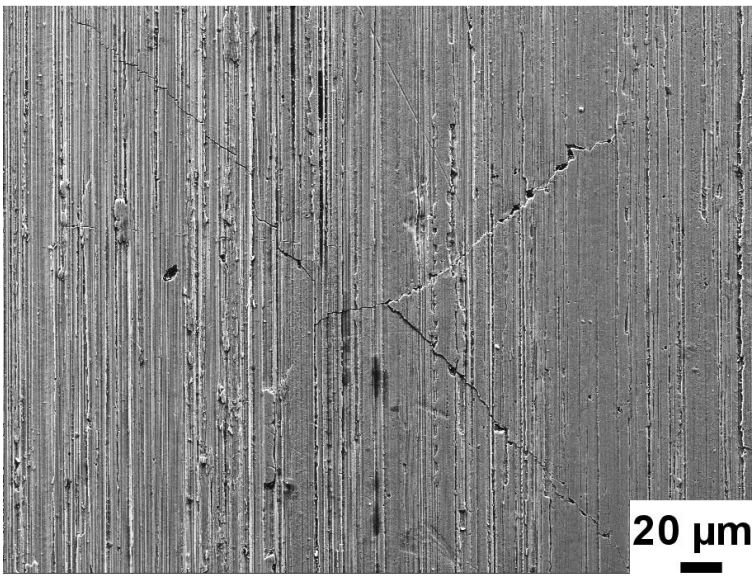

Figure 8. SEM image showing an X-shape crack near the groove in the pit-free sample.

4. Conclusions and outlook

A test rig has been constructed at the Department of Mechanical Engineering at the Technical University of Denmark and it has been shown that the rig can be effectively used for studies of rolling contact fatigue of bearing steels under well-controlled conditions. In this test rig, the loading on the rings can be adjusted to obtain a specified maximum contact pressure, and the rotational speed of the contacting rings can be adjusted to obtain specified slip conditions. The circumferential stress in the rings can be achieved by adjusting the axial ring position on the conical shaft.

Initial results using the test rig on samples taken from two spherical roller bearings using rings of 3 mm and 5 mm width lead to the following conclusions:

- Rolling contact fatigue testing under a high load results in pitting failure at the contacting surfaces. Pitting was preferably observed on one side of the contact, attributed to a non-uniform contact pressure along the axial direction. Due to the conical shape of the contacting ring surfaces the contact pressure along the line contact was sufficiently high so that plastic deformation occurred, indicated by the fact that the 3-mm wide ring produced a groove in the 5-mm wide ring.
- A progression in damage at the contact surface, stemming from the grinding process used in the present experiment, was observed over several thousand revolutions of the test piece, finally resulting in severe vibrations. This situation is also typical in wind turbine applications, where manufacturing defects and misalignments can lead to premature failures of the roller bearings in gear boxes.

Future work will include experiments with different loads and slippage conditions.

Acknowledgement

The work was supported by the Strategic Research Center "REWIND – Knowledge based engineering for improved reliability of critical wind turbine components", grant no. 10-093966 from the Danish Research Council for Strategic Research.

References

[1] http://evolution.skf.com/us/new-challenges-for-rotor-bearings-in-the-8-mw-offshore-category
[2] LaCava W, Keller J and McNiff B 2012 Gearbox reliability collaborative: test and model investigation of sun orbit and planet load share in a wind turbine gearbox. *53rd Structures, Structural Dynamics and Materials Conference* (Honolulu, Hawaii)
[3] Guo Y, Bergua R, van Dam J, Jove J and Campbell J. (2015) *Wind Energy* **18** 2199
[4] IEC 61400-4. Wind turbines - Part 4: Design requirements for wind turbine gearboxes 2012 *International Electrotechnical Commision*
[5] IEC 61400-1. Wind turbines - Part 1: Design of wind turbines, Edition 3 2005 *International Electrotechnical Commision*
[6] Dabrowski D and Natarajan A 2017 *Wind Energy* DOI: 10.1002/we.2098
[7] Gallego Calderon J F, Natarajan A and Cutululis N A. 2017 *Wind Energy* **20** 325
[8] Klit P, Casper K and Pedersen N L. *Machine Elements Analysis and Design.* Polyteknisk Forlag, Kgs. Lyngby, First edition, 2009
[9] Feldkamp L A, Davis L C and Kress J W 1984 *J Opt Soc Am A* **1** 612